Low-energy proton–hydrogenlike-ion scattering in the Coulomb-Born approximation

J. E. Potter and J. Macek
Department of Physics and Astronomy, University of Nebraska-Lincoln, Lincoln, Nebraska 68588
(Received 18 May 1979)

Excitation probabilities for the $1s$-$2s$ transition of hydrogenlike ions by low-energy $(4-100)E_{\text{th}}$ protons are calculated in the Coulomb-Born approximation and compared to the corresponding calculations in the semiclassical approximation with hyperbolic trajectories. Through the use of a Fourier-Bessel transform, an effective energy is derived for the semiclassical approximation, which brings the total cross section into agreement with the Coulomb-Born results.

I. INTRODUCTION

Recent experimental and theoretical studies of inner-shell ionization of heavy targets by low-energy protons[1-6] have shown that relativistic corrections to semiclassical calculations are important. The necessity for such corrections is especially noticeable at large scattering angles.[6] That this is true for large angles may be qualitatively explained as follows. In order to have a significant number of excitations of K-shell electrons, the electrons must be subjected to a time-varying electric field with Fourier components ω, such that

$$\hbar\omega = \Delta E\,, \tag{1}$$

where ΔE is the excitation energy. Such a field is produced by slow protons if their trajectory makes an abrupt change, i.e., for collisions with small impact parameters where the trajectory's point of closest approach is near the nucleus. Alternatively, the high Fourier coefficients are obtained when the energy exchange is large. For slow protons, this implies a large momentum change as well and occurs when the scattering angle is large. Since the electron velocities in this region are large, the relativistic corrections to the electron wave functions noticeably affect the excitation cross sections. This offers the possibility that low-energy inelastic proton scattering could be used as a dynamic probe to investigate relativistic corrections to atomic wave functions. However, before such a probe can be exploited, the magnitude of other sources of uncertainties in the theory should be considered.

In this paper we study one of these: the uncertainty attributable to the use of the semiclassical approximation in calculations of total and differential cross sections. The use of the semiclassical approximation is justified for high incident energies, but is incorrect for extremely low incident proton energies. In particular, because the proton loses as much as 10%–20% of its energy in low-energy inelastic collisions, it cannot be said to follow a classical trajectory. A better description of the scattering is obtained by the use of Coulomb wave functions for the incident proton. In this study, we proceed by calculating the probabilities for the inelastic excitation of hydrogenlike ions by low-energy protons in the CBA (Coulomb-Born approximation) and comparing this calculation with the SCA (semiclassical approximation) calculation. We consider $1s$-$2s$ excitation as a model study, since s-s transitions are the most significant contribution to inelastic scattering for slow protons. We note that the use of a scaling factor for cross sections and energy makes the numerical results presented in this paper applicable to a wide range of Z. This is possible because we use the unscreened Coulomb potential; thus the curve $Z^2\sigma$ vs E/Z^2 is universal. Here the energy, and all other quantities in this work, are determined in the center-of-mass frame.

In Sec. II we present the necessary formalism for the calculation of differential excitation probabilities and total cross section using both the CBA and the SCA for the process

$$H^+ + A^{(Z-1)+}(1s) \rightarrow H^+ + A^{(Z-1)+}(2s)\,. \tag{2}$$

Numerical results are presented and discussed in Sec. III for He^+ targets for the energy range (4–100) times the threshold energy. In addition, we compare the CBA and SCA by means of a Bessel transform and derive an effective energy for the SCA. This effective energy permits one to use the SCA for total cross-section calculations at low energies with relatively small errors. Conclusions are presented in Sec. IV.

II. FORMALISM

A. Coulomb-Born approximation

Oh *et al.*[7] have obtained closed form expressions for transition matrix elements for inelastic electron–hydrogenlike-ion collisions in the CBA. With suitable minor changes, we can apply their results

to inelastic proton–hydrogenlike-ion scattering.

The Hamiltonian for the incident proton is taken to be

$$\mathcal{H} = T + Ze^2/r\,, \tag{3}$$

where we assume that the screening by the orbital electron is negligible because the proton penetrates to a region near the nucleus. The incoming and outgoing wave functions for the proton in terms of hypergeometric functions are[8]

$$\psi_{\vec{k}}^{(+)}(\vec{r}) = N_k^{(+)}\, e^{i(\vec{k}\cdot\vec{r})}\, {}_1F_1(+a, 1; i(kr - \vec{k}\cdot\vec{r})) \tag{4}$$

and

$$\psi_{\vec{k}'}^{(-)}(\vec{r}) = N_{k'}^{(-)}\, e^{i(\vec{k}'\cdot\vec{r})}\, {}_1F_1(-b, 1; -i(k'r + \vec{k}'\cdot\vec{r}))\,, \tag{5}$$

where the normalization is to unit amplitude, with the normalization constants defined by

$$N_k^{(+)} = \exp(-\tfrac{1}{2}i\pi a)\,\Gamma(1-a) \tag{6}$$

and

$$N_k^{(-)} = \exp(-\tfrac{1}{2}i\pi b)\,\Gamma(1+b)\,. \tag{7}$$

The initial and final wave vectors are $\vec{k}$ and $\vec{k}'$, respectively, and we define

$$a = -iZM/k \tag{8}$$

and

$$b = -iZM/k'\,; \tag{9}$$

M is the reduced mass of the system, and Z is the atomic number of the target.

The inelastic scattering amplitude[9] is given by

$$A_{i\to f} = \frac{-M}{2\pi}\int d^3r\, \psi_{\vec{k}'}^{(-)*}(\vec{r})\, U_{if}(\vec{r})\, \psi_k^{(+)}(\vec{r})\,. \tag{10}$$

Here, $U_{if}(\vec{r})$ is the matrix element of the hydrogenic wave functions with the potential $e^2/|\vec{r}-\vec{r}'|$:

$$U_{if}(\vec{r}) = \int d^3r'\, \varphi_f^*(\vec{r}\,')\, \frac{e^2}{|\vec{r}-\vec{r}'|}\, \varphi_i(\vec{r}\,')\,. \tag{11}$$

For the $1s \to 2s$ excitation, this is readily integrated to obtain

$$U_{1s,2s} = (\tfrac{4}{27}\sqrt{2}Z)(1+\tfrac{3}{2}Zr)e^{-3Zr/2}\,. \tag{12}$$

Now, using the results of Ref. 7, we find

$$A_{1s\to 2s} = \frac{2\sqrt{2}}{27\pi} ZMN_k^{(+)} N_{k'}^{(-)} \left(1 - X\frac{\partial}{\partial X}\right)\frac{\partial}{\partial X} I_{ab}\,, \tag{13}$$

where

$$I_{ab} = 4\pi[X^2 + (\vec{k}-\vec{k}')^2]^{a+b-1}[X - i(k-k')]^{-(a+b)}(X - ik + ik')^{-a}(X + ik - ik')^{-b}\, {}_2F_1\left(a, b; 1; 1 - \frac{X^2 + (\vec{k}-\vec{k}')^2}{X^2 + (k-k')^2}\right) \tag{14}$$

and

$$X = \tfrac{3}{2}Z\,. \tag{15}$$

We use atomic units throughout this work, so this scattering amplitude is related to the differential cross section by the expression

$$\sigma(E,\Omega) = (k'/k)|A_{i\to f}|^2\,. \tag{16}$$

To facilitate comparison with the SCA calculation, we prefer to use the excitation probability rather than the cross section. We obtain the probability by dividing the CBA differential cross section by the Rutherfold cross section for the same energy and angle. This is justifiable in our calculations since the elastic scattering is the primary component in the total cross section at a given angle.

Numerical results were obtain for the process

$$H^+ + He^+(1s) \to H^+ + He^+(2s) \tag{17}$$

at various energies and are discussed in Sec. III.

B. Semiclassical approximation

The purpose of this section is to obtain an expression for the excitation probability for the process described by Eq. (2) with the assumption that the incident proton follows a classical hyperbolic trajectory.

The parameters necessary to describe hyperbolic trajectories have been given by Landau and Lifshitz.[10] Methods of evaluating the integrals involved have been reviewed by Kocbach[11] in a discussion of the general theory of the SCA. The definition and method that we used to obtain an expression for the excitation probability are summarized as follows. The probability amplitude for excitation a_{if}, is given in terms of the time-dependent classical trajectory $R(t)$, by

$$a_{if} = -i\int_{-\infty}^{\infty} U_{if}(R(t))e^{-i\Delta Et}\,dt\,, \tag{18}$$

where the quantity U_{if} is the same as in the CBA shown by Eq. (12). The classical trajectory and the time are expressed in terms of the parameter Ω by

$$R(\Omega) = (Z/2E)(\epsilon\cosh\Omega + 1) \tag{19}$$

and

$$t = (Z/2Ev)(\epsilon\sinh\Omega + \Omega)\,. \tag{20}$$

Here, E is the energy and ϵ is the eccentricity of the hyperbolic path. It is related to the impact parameter B by the equation

$$\epsilon = [1 + (2EB/Z)^2]^{1/2}\,. \tag{21}$$

In terms of the scattering angle, B is found to be

$$B = (Z/2E)\cot(\tfrac{1}{2}\theta)\,. \tag{22}$$

We also define the quantities

$$C = Z/2E\,, \tag{23}$$

and

$$\omega = \Delta E/v\,. \tag{24}$$

After making some obvious substitutions, we find the excitation amplitude to be

$$a_{1s,2s} = -\frac{i4\sqrt{2}Z}{27v}\int_{-\infty}^{\infty} R(1+XR)e^{-XR} \times \exp[-i\omega C(\epsilon\sinh\Omega+\Omega)]\,d\Omega\,, \tag{25}$$

where $X = \frac{3}{2}Z$.

To evaluate the amplitude in Eq. (25), we consider the integral

$$I = \int_{-\infty}^{\infty} R^2 e^{-XR}\exp[-i\omega C(\epsilon\sinh\Omega+\Omega)]\,d\Omega\,, \tag{26}$$

$$= C^2\int_{-\infty}^{\infty}(\epsilon^2\cosh^2\Omega + 2\epsilon\cosh\Omega + 1)\exp[-XC(\epsilon\cosh\Omega+1)]\exp[-i\omega C(\epsilon\sinh\Omega+\Omega)]\,d\Omega\,. \tag{27}$$

This is separated into the three integrals

$$I_0 = \int_{-\infty}^{\infty}\exp[-XC(\epsilon\cosh\Omega+1)]\exp[-i\omega C(\epsilon\sinh\Omega+\Omega)]\,d\Omega\,, \tag{28}$$

$$I_1 = \int_{-\infty}^{\infty}\cosh(\Omega)\exp[-XC(\epsilon\cosh\Omega+1)]\exp[-i\omega C(\epsilon\sinh\Omega+\Omega)]\,d\Omega\,, \tag{29}$$

$$I_2 = \int_{-\infty}^{\infty}\cosh(2\Omega)\exp[-XC(\epsilon\cosh\Omega+1)]\exp[-i\omega C(\epsilon\sinh\Omega+\Omega)]\,d\Omega\,. \tag{30}$$

Defining the quantity ϕ by the relations

$$\cos\varphi = X/(X^2+\omega^2)^{1/2} \tag{31}$$

and

$$\sin\varphi = \omega/(X^2+\omega^2)^{1/2}\,, \tag{32}$$

and with the transformation

$$\Omega' = \Omega + i\varphi\,, \tag{33}$$

we can integrate I_0, I_1, and I_2 analytically. The results for these integrals are given in closed form by modified Bessel functions of the third kind[11]:

$$I_0 = 2e^{-XC}e^{-\omega C\varphi}K_{i\omega C}(C\epsilon(X^2+\omega^2)^{1/2})\,, \tag{34}$$

$$I_1 = e^{-XC}e^{-\omega C\varphi}[e^{-i\varphi}K_{-1+i\omega C}(C\epsilon(X^2+\omega^2)^{1/2}) + e^{i\varphi}K_{1+i\omega C}(C\epsilon(X^2+\omega^2)^{1/2})]\,, \tag{35}$$

and

$$I_2 = e^{-XC}e^{-\omega C\varphi}[e^{-2i\varphi}K_{-2+i\omega C}(C\epsilon(X^2+\omega^2)^{1/2}) + e^{2i\varphi}K_{2+i\omega C}(C\epsilon(X^2+\omega^2)^{1/2})]\,. \tag{36}$$

We find that the integral

$$\int_{-\infty}^{\infty} R\,e^{-XR}\exp[-i\omega C(\epsilon\sinh\Omega+\Omega)]\,d\Omega \tag{37}$$

can be simply written in terms of I_0 and I_1. Thus when the preceding equations are used with Eq. (25), we have the excitation amplitude given by the relatively simple expression

$$a_{1s,2s} = (-i4\sqrt{2}Z/27v)[(C+\tfrac{1}{2}C^2X\epsilon^2+XC^2)I_0 + (C\epsilon+2C^2\epsilon X)I_1 + \tfrac{1}{2}C^2\epsilon^2XI_2] \tag{38}$$

for the $1s \to 2s$ transition. The desired probability is then simply

$$P(1s\to 2s) = a_{1s,2s}a^*_{1s,2s}\,. \tag{39}$$

III. RESULTS AND DISCUSSION

In this section we report the numerical results obtained for the process described by Eq. (17) for both the CBA and the SCA over the energy range (4–100) times the threshold energy ($E_{\rm th} = 1.5$ a.u.).

The hypergeometric functions necessary for the CBA calculations were accurately evaluated by computer using a series approximation with appropriate transformations of the argument to assure rapid convergence.[12] The modified spherical Bessel functions of the third kind (MacDonald functions) $K_\nu(Z)$ occurring in the SCA formulas were evaluated from the relation

$$K_\nu(Z) = [\pi/2\sin(\pi\nu)][I_{-\nu}(Z) - I_\nu(Z)]\,, \quad (\nu \neq 0, 1, 2, \ldots) \tag{40}$$

where $I_\nu(Z)$ is the modified Bessel function of the first kind.[12] Values of $I_\nu(Z)$ and $I_{-\nu}(Z)$ were obtained from a series expansion. We note that for small energies the values of $I_\nu(Z)$ and $I_{-\nu}(Z)$ are

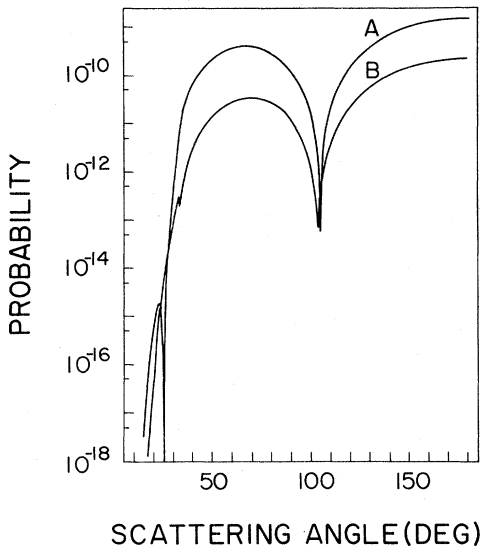

FIG. 1. Differential excitation probability vs angle for $E/E_{th}=5$. Curve labeled A is the SCA result; curve labeled B is the CBA result.

quite large and very close in value, thus care must be taken in evaluating $K_\nu(Z)$.

A. Differential excitation probabilities

The results of the calculations of differential excitation probabilities are illustrated in Figs. 1–4. These particular energies were chosen because the shape of the probability versus scattering angle curves are typical for those energy regions.

The shapes of the curves in Fig. 1 are similar to those obtained from the lowest energy considered for CBA ($E=3E_{th}$) up to approximately $8E_{th}$. The deep minima near 103°–105° in this figure are present in all the probability curves for this energy range, although the minima shift toward larger angles as the energy increases. Mathematically, these minima occur because at low energies in both the CBA and SCA, the probability is obtained by summing large complex numbers that are slightly out of phase. This effect is physical as well. In the SCA case the variation of probability with angle is attributed to the interference of incoming and outgoing amplitudes[6]; in the CBA case the interference (at low energies) is between the incoming and outgoing Coulomb waves for the incident proton. We particularly note that the scattering has a higher probability for large angles in this energy range.

In Figs. 2 and 3, one can see the gradual disappearance of the minima, and an increase in the component of scattering at smaller angles. The magnitude of the probability increases as the energy increases, a relationship that is true over the entire energy range we studied.

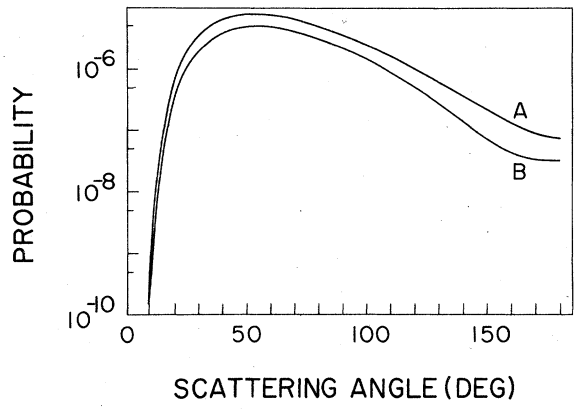

FIG. 3. Differential excitation probability vs angle for $E/E_{th}=10$. Curve labeled A is the SCA result; curve labeled B is the CBA result.

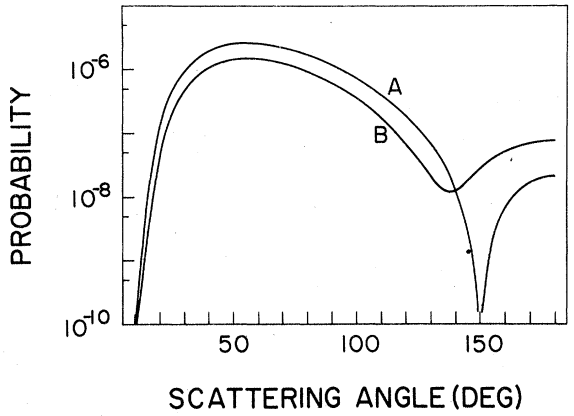

FIG. 2. Differential excitation probability vs angle for $E/E_{th}=9$. Curve labeled A is the SCA result; curve labeled B is the CBA result.

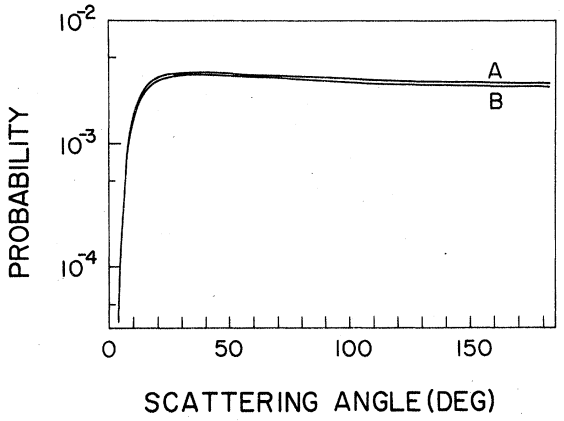

FIG. 4. Differential excitation probability vs angle for $E/E_{th}=30$. Curve labeled A is the SCA result; curve labeled B is the CBA result.

TABLE I. Probabilities of excitation for scattering angle of 180°.

Energy (E/E_{th})	Probability (SCA)	Probability (CBA)	Difference (%)
5	1.525×10^{-9}	2.2418×10^{-10}	580
6	1.795×10^{-8}	6.565×10^{-9}	170
7	6.370×10^{-8}	4.061×10^{-8}	57
8	8.666×10^{-8}	9.180×10^{-8}	−5.6
9	2.199×10^{-8}	7.913×10^{-8}	−72
10	7.428×10^{-8}	3.242×10^{-8}	130
12	4.441×10^{-6}	2.528×10^{-6}	76
15	5.337×10^{-5}	4.090×10^{-5}	31
20	4.341×10^{-4}	3.829×10^{-4}	13
30	3.087×10^{-3}	2.940×10^{-3}	5.0
50	1.551×10^{-2}	1.529×10^{-2}	1.5
100	5.874×10^{-2}	5.867×10^{-2}	0.12

In tne energy range beyond $10E_{th}$ the shape of the probability curves rapidly approaches that shown in Fig. 4, with the SCA curves always higher than, but getting closer to, the CBA curves as the energy increases. Since we are particularly interested in scattering at large angles, in Table I we compare the probabilities for excitation at a scattering angle of 180° with the difference D calculated as

$$D = 100\frac{P^{SCA} - P^{CBA}}{P^{CBA}}\% . \tag{41}$$

The difference appears erratic at the lower energies, due primarily to the phase differences in the amplitudes. This is considered in more detail later.

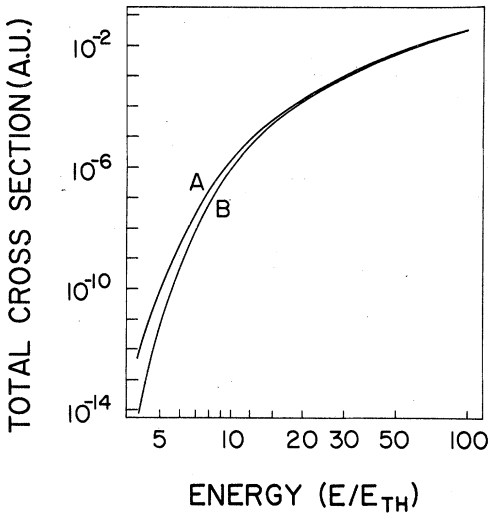

FIG. 5. Total cross sections. Curve A is the SCA result; curve B is the CBA result. Both are in a.u.

B. Total cross section

The total cross section was obtained by numerically integrating over the differential excitation probabilities in the usual way. As would be expected, the agreement is very good for relatively high energies, with the SCA total cross section being too large at low energies, as shown in Fig. 5. The uniformity of the difference between the two curves suggests that an energy-dependent correction might improve the SCA results. Such a correction is derived through the analysis in Sec. II C. The total cross sections obtained from the SCA and CBA are presented in Table II.

TABLE II. Total cross section for CBA, SCA, and SCA (corrected) in a.u.

Energy (E/E_{th})	σ_{tot}^{CBA}(a.u.)	σ_{tot}^{SCA}(a.u.)	Difference from CBA (%)	$\sigma_{tot}^{SCA'}(E-\Delta E/\nu)$	Difference from CBA (%)
4.0	8.551×10^{-15}	5.940×10^{-13}	6900	...	...
5.0	8.565×10^{-12}	1.016×10^{-10}	1100	1.230×10^{-11}	44
6.0	5.480×10^{-10}	2.907×10^{-9}	430	6.341×10^{-10}	16
7.0	9.301×10^{-9}	2.937×10^{-8}	220	1.020×10^{-8}	9.6
7.5	2.700×10^{-8}	7.325×10^{-8}	170	2.937×10^{-8}	8.8
8.0	6.690×10^{-8}	1.622×10^{-7}	140	7.325×10^{-8}	9.5
8.5	1.482×10^{-7}	3.227×10^{-7}	120	1.622×10^{-7}	9.4
9.0	2.966×10^{-7}	5.927×10^{-7}	100	3.227×10^{-7}	8.8
9.5	5.518×10^{-7}	1.023×10^{-6}	86	5.927×10^{-7}	7.4
10.0	9.744×10^{-7}	1.667×10^{-6}	71	1.023×10^{-6}	5.0
12.0	5.302×10^{-6}	7.766×10^{-6}	47	5.534×10^{-6}	4.4
15.0	2.837×10^{-5}	3.629×10^{-5}	28	2.930×10^{-5}	3.3
20.0	1.550×10^{-4}	1.811×10^{-4}	17	1.589×10^{-4}	2.5
30.0	9.774×10^{-4}	1.069×10^{-3}	9.4	9.986×10^{-4}	2.2
50.0	5.595×10^{-3}	5.806×10^{-3}	3.8	5.644×10^{-3}	0.88
100.0	2.931×10^{-2}	2.951×10^{-2}	0.72	2.924×10^{-2}	−0.23

C. Effective energy for the SCA

In this section we express the scattering amplitudes for both the SCA and CBA calculation in similar forms. This is important because from a comparison of these expressions, parameters for the SCA are established that are analogous to those of the CBA formalism. Thus, by equating these parameters, we find an equivalent energy for the SCA calculation which produces results for the total cross section that are in good agreement with the CBA results.

As shown by Wilets and Wallace[13] and others[14] the semiclassical probability amplitude $a_{if}(b)$, and the inelastic scattering amplitude $A_{if}^{\mathrm{SCA}}(\theta)$ are related by the Fourier-Bessel transform

$$A_{if}^{\mathrm{SCA}}(\theta) = Mv \int_0^\infty a_{if}(b) J_m[2Mvb \sin(\tfrac{1}{2}\theta)] b \, db \,. \tag{42}$$

This relation was obtained from Eq. (51) of Ref. 13, with modifications appropriate to scattering via a strong Coulomb potential.[13] Equation (42) indicates that evaluation of the pertinent Bessel transforms would permit a comparison of the CBA and SCA expressions for A_{if}. Since the amplitudes are obtained by linear operations on I_{ab}, we need consider only I_{ab} and its semiclassical analog.

Using Eq. (6.576-3) of Ref. 15 we may write an amplitude A^{CBA} as

$$\begin{aligned} A^{\mathrm{CBA}} &\equiv -(M/2\pi) N_k^{(+)} N_{k'}^{(-)*} I_{ab} \\ &= 2\left(\frac{4}{(k+k')^2+X^2}\right)^{-(a+b)/2} \exp[\tfrac{1}{2}i\pi(a-b)] \exp\left[-i(a+b)\arctan\left(\frac{X}{k+k'}\right) - i(a-b)\arctan\left(\frac{X}{k-k'}\right)\right] \\ &\quad \times M \int_0^\infty t^{1-a-b} K_{a-b}\{[X^2+(k-k')^2]^{1/2} t\} J_0[2M(vv')^{1/2} \sin(\tfrac{1}{2}\theta) t] \, dt \,. \end{aligned} \tag{43}$$

To write Eq. (43) into a functional form similar to Eq. (42), we define

$$\begin{aligned} \omega' &= 2\Delta E(v+v') \,, \\ C' &= -Z/Mvv' \,, \\ \phi' &= -\tfrac{1}{2}\pi + \arctan[X/M(v-v')] = -\arctan(\omega'/X) \,. \end{aligned} \tag{44}$$

In addition, since $X^2/(k+k')^2$ is on the order of 10^{-4} or smaller, we neglect terms of this order to obtain

$$\begin{aligned} A^{\mathrm{CBA}} \approx & \left(\frac{2}{k+k'}\right)^{-(a+b)} \exp(-XC' - \omega' C' \phi') Mv \\ & \times \left(v^{-1} \int_0^\infty t^{1-a-b} K_{i\omega' C'}[(X^2+\omega'^2)^{1/2} t] \right. \\ & \left. \times J_0[2M(vv')^{1/2} \sin(\tfrac{1}{2}\theta) t] \, dt \right). \end{aligned} \tag{45}$$

Except for the phase factor $[2/(k+k')]^{-(a+b)}$, this expression is similar to Eq. (42), with $a_{if}(b)$ corresponding to I_{ab}/v. The most significant difference is that t in Eq. (45) replaces ϵ in Eq. (34); this is necessary to obtain agreement between the SCA and CBA total cross sections.

In order to see this, we define

$$y = 2M(vv')^{1/2} \sin(\tfrac{1}{2}\theta) \,, \tag{46}$$

and note that because Bessel transforms preserve normalization, we have

$$\begin{aligned} \int_0^\infty |A^{\mathrm{CBA}}|^2 y \, dy = & M^2 v^2 \exp(-2XC' - 2\omega' C' \phi') \\ & \times \int_0^\infty |K_{i\omega' C'}[(X^2+\omega'^2)^{1/2} t]|^2 t \, dt \,. \end{aligned} \tag{47}$$

Now since $(v/v')y \, dy = M^2 v^2 \sin\theta \, d\theta$, we see that the integration over y on the left-hand side of Eq. (47) includes nonphysical regions where $\sin(\frac{1}{2}\theta)$ is greater than unity. This corresponds to the forbidden region where $\epsilon < 1$. We exhibit this region by defining an impact parameter B', such that

$$B'^2 = t^2 - Z^2/4E^2 \,. \tag{48}$$

Upon substitution of this expression, Eq. (47) becomes

$$\int_0^\infty |A^{\mathrm{CBA}}|^2 y \, dy = 2M^2 v^2 \exp[-2XC' - 2\omega' C' \phi'] \int_{-Z^2/4E^2}^\infty \left| v^{-1} K_{i\omega' C'}\left[(X^2+\omega'^2)^{1/2}\left(B'^2 + \frac{Z^2}{4E^2}\right)^{1/2}\right] \right|^2 d(B'^2) \,. \tag{49}$$

In this form, the integrations in Eq. (49) include some nonphysical regions of y on the left-hand side and B' on the right-hand side. Now we limit the integration on the left-hand side to physical values of $y < 2M(vv')^{1/2}$, and compensate for the error introduced by this by taking zero as the lower limit on the right-hand side. [That the errors do indeed compensate is seen by noting that for a Coulomb potential where the relation $y = 2Mv/(1+4E^2B'^2/Z^2)^{1/2}$ holds, the region $2Mv \leq y < \infty$ corresponds exactly with the region $0 \leq B'^2 < -Z^2/4E^2$.] Recalling that

$$(v/v')y \, dy = M^2 v^2 \sin\theta \, d\theta \,,$$

we have

$$\frac{v'}{v}\int_0^{\pi}|A^{\mathrm{CBA}}|^2\sin\theta\,d\theta$$
$$\approx\exp[-2XC'-2\omega'C'\phi']2\int_0^{\infty}\left|v^{-1}K_{i\omega'C'}\left[(X^2+\omega'^2)^{1/2}\left(B'^2+\frac{Z^2}{4E^2}\right)^{1/2}\right]\right|^2 B'\,dB'=\int_0^{\infty}|A^{\mathrm{SCA}}|^2B'\,dB'\,. \tag{50}$$

Now in Eq. (50) we have the integrated CBA amplitude on the left-hand side of the equal sign expressed in terms of the corresponding analogous SCA amplitude on the right-hand side. Thus we see that the integrated CBA and SCA expressions agree to the extent that $\omega'=\omega$ and $C'=C$. We note that the approach of the approximate expression in Eq. (50) to an equality depends quite sensitively on the index $\omega'C'$, since the magnitude of K_ν depends upon cancellation of I_ν and $I_{-\nu}$ [see Eq. (40)]. Accordingly, we propose that SCA cross sections be calculated for an effective energy E_{eff}, such that $\omega'C'=\omega C$. To find E_{eff}, we simply write $\omega'C'=\omega C$ explicitly in terms of E_{eff} to obtain

$$Z\Delta E/2v_{\mathrm{eff}}E_{\mathrm{eff}}=2Z\Delta E/Mvv'(v+v')\,, \tag{51}$$

With the approximation $v'\simeq v-\Delta E/(4vM)$, and using $v_{\mathrm{eff}}=(2E_{\mathrm{eff}}/M)^{1/2}$, we find

$$E_{\mathrm{eff}}\approx E-\tfrac{1}{2}\Delta E\,. \tag{52}$$

This means that one obtains a good approximation to the CBA result for the total cross section at low energies by using the computationally simpler SCA equations at the lower energy E_{eff}. Specifically, the modified Bessel functions K_ν present fewer problems numerically than the hypergeometric functions ${}_2F_1$. This results in the SCA calculation using approximately one-fourth as much computer time as the CBA calculation for total cross section.

In Fig. 6, the CBA cross section (curve B) is compared with the energy-shifted SCA cross section (dashed curve). One can see easily the greatly improved agreement between the two calculations. This is seen more accurately in Table II, The energy-shifted SCA cross section agrees to within 10% of the CBA cross section for energies above seven times the threshold energy, in contrast to the 200% difference for the unshifted result.

A prescription frequently given[16] for correcting the SCA is to introduce an effective velocity $v_{\mathrm{eff}}=\frac{1}{2}(v+v')$, with the corresponding effective energy $E-\frac{1}{4}\Delta E$. Our derivation, and the results in Table II, show this to be in error: rather, one should use the effective energy in Eq. (52).

The effective energy of Eq. (51) is chosen to obtain equality of the total cross sections; however, a stationary phase evaluation of the Bessel transform of Eq. (45) suggests that the angular distribution results might be improved as well. Figure 7 compares the CBA probability at $\theta=\pi$ (curve B), with the energy-shifted SCA results (dashed curve). We see that above $E=12E_{\mathrm{th}}$ the shifted curve represents an improvement over the unshifted curve A, although there is still a noticeable difference. In fact, it overcorrects the cross section for large angles, and it does not provide a good description near $E=10E_{\mathrm{th}}$. Above $E=30E_{\mathrm{th}}$,

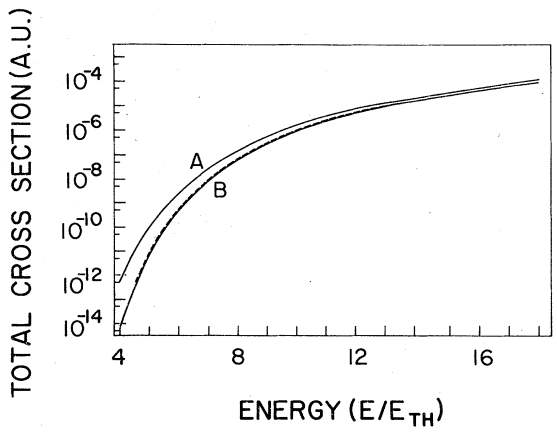

FIG. 6. Total cross sections with energy shifted SCA result. Solid curve A is the SCA; dashed curve is the energy shifted SCA, and solid curve B is the CBA result.

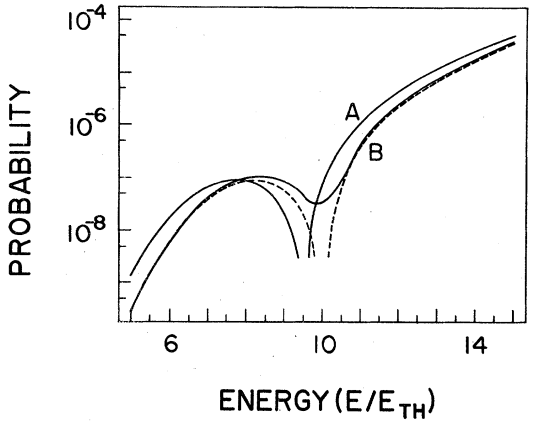

FIG. 7. Excitation probabilities for $\theta=\pi$ as a function of energy. Curve A is the SCA result, solid curve B is the CBA result, and the dashed curve is the energy-shifted SCA result.

the unshifted results are actually better. In view of the indifferent agreement between the CBA and the energy shifted SCA angular distribution, there is little reason to prefer one version of the SCA over the other. Below $30E_{th}$ a full wave treatment is needed for a consistent picture of the angular distribution.

IV. CONCLUSIONS

We have presented the SCA and CBA approximations for the $1s$-$2s$ inelastic excitation cross section, and as an example we report numerical results for He^+ at low incident proton energies. This calculation is intended as a prototype of low-energy inelastic excitation processes in proton-atom collisions. The numerical results obtained may be used to determine the cross sections for hydrogenlike ions of different Z by the use of a scaling factor. We find that SCA total cross sections calculated at an effective energy are reliable at all energies of practical interest. However, angular distributions require a full wave treatment below $E = 30E_{th}$. Since this is the region where relativistic effects are most important, it is desirable to employ a full wave treatment with relativistic wave functions.

ACKNOWLEDGMENTS

This work was supported by the National Science Foundation under Grant No. PHY77-07110.

[1]P. A. Amundsen and L. Kocbach, J. Phys. B 8, L122 (1975).
[2]L. Kocbach, Z. Phys. A 279, 233 (1976).
[3]A. Berinde, C. Deberth, I. Neamu, C. Protop, N. Scintei, V. Zoran, M. Dost, and S. Röhl, J. Phys. B 11, 2875 (1978).
[4]P. A. Amundsen, L. Kocbach, and J. M. Hansteen, J. Phys. B 9, L203 (1976).
[5]O. Aashamar and L. Kocbach, Z. Phys. A 279, 237 (1976).
[6]J. U. Andersen, L. Kocbach, E. Laegsgaard, M. Lund, and C. D. Moak, J. Phys. B 9, 3247 (1976).
[7]S. D. Oh, J. Macek, and E. Kelsey, Phys. Rev. A 17, 873 (1978).
[8]L. D. Landau and E. M. Lifshitz, *Quantum Mechanics*, 2nd ed. (Pergamon, New York, 1965).
[9]In Ref. 7 this amplitude was referred to as a transition matrix element. Such a designation is confusing since Eq. (10) does not employ any of the standard T-matrix normalizations. The normalization used in Eq. (10) corresponds to that used for scattering amplitude; therefore, in this paper we use A_{if} to denote such inelastic scattering amplitudes.
[10]L. D. Landau and E. M. Lifshitz, *Classical Mechanics* (Pergamon, New York, 1960).
[11]L. Kocbach, Phys. Norv. 8, 187 (1976).
[12]M. Abramowitz and I. A. Stegun, *Handbook of Mathematical Functions*, NBS Applied Mathematics Ser. 55 (National Bureau of Standards, Washington, D.C., 1964).
[13]L. Wilets and S. J. Wallace, Phys. Rev. 169, 84 (1968).
[14]R. McCarroll and A. Salin, J. Phys. B 1, 163 (1968).
[15]I. S. Gradshteyn and I. M. Ryzhik, *Table of Integrals, Series, and Products* (Academic, New York, 1965).
[16]K. Alder and A. Winther, *Coulomb Excitation* (Academic, New York, 1966).